Materials Advances

ROYAL SOCIETY OF CHEMISTRY

PAPER

View Article Online
View Journal | View Issue

Cite this: *Mater. Adv.*, 2025, 6, 2611

Enhanced photocatalytic efficiency of eco-friendly synthesized ZnO for rapid full degradation of methylene blue dye

Mohammad Tashakkori Masuleh, Masood Hasheminiasari and Rouholah Ashiri *

Received 10th January 2025,
Accepted 17th March 2025

DOI: 10.1039/d5ma00026b

rsc.li/materials-advances

The rapid advancement of industry and economic development have enhanced productivity, urbanization, and living standards; but uncontrolled emissions of pollutants from various industries have adversely affected the environment. Organic dyes in industrial wastewater represent a significant source of pollution, causing serious risks to aquatic environments and public health due to their high stability and resistance to breakdown. An effective strategy for eliminating these contaminants is the application of photocatalytic semiconductors like ZnO. In this study, ZnO nanoparticles were synthesized *via* a modified sol–gel method utilizing three different solvents (ethanol, 1-propanol and 1,4-butanediol), investigating the influence of solvent type on their structural and photocatalytic characters. The results indicate that the samples synthesized with ethanol exhibit superior photocatalytic efficacy in the degradation of methylene blue (MB), achieving a pollutant elimination efficiency of 98% within a brief duration. This study demonstrates that selecting an appropriate solvent substantially influences the final characteristics of ZnO leading to a marked enhancement in its photocatalytic efficacy.

1. Introduction

The rapid process of industrialization and economic advancement have resulted in increased productivity, urbanization and an overall improvement in living standards. Nevertheless, the uncontrolled release of contaminants from many industries has resulted in detrimental effects on the biosphere.[1] In many industries including paper, dyeing, textiles, plastics, cosmetics, and pharmaceuticals, the broad use of organic dye molecules results in the release of harmful, non-biodegradable industrial effluents into the environment in the absence of adequate treatment. The release of dye-contaminated wastewater has considerable environmental risks, affecting ecosystems and public health.[2] Organic dye pollutants from industrial sources adversely affect aquatic ecosystems and modify water quality. Azo dyes, characterized by –N=N– bonds, are pH-dependent and display amphoteric properties. Additionally, they are highly stable, poisonous and challenging to degrade.[3]

The use of semiconductors to facilitate the photocatalytic elimination of resistant compounds is an advantageous and economically viable method. This is because semiconductors have the ability to function effectively under various reaction settings.[4] Photocatalytic methods offer several benefits, including the capacity to adjust to different temperatures and ambient conditions, the utilization of sunlight to initiate and complete the reaction, and the possibility of reusing photocatalyst particles.[5]

Binary semiconductors, such as TiO_2, ZnO, Fe_2O_3, WO_3, Bi_2O_3, CuO_2, CdS, and ZnS, are commonly used as photocatalysts. This is due to their favorable combination of electronic structure, light absorption characteristics, charge transfer characteristics, and excited state lifetime. Additionally, they are low-cost and have high quantum efficiency. These semiconductors are also chosen for their favorable energy gap and photocatalytic mechanisms[6,7]

Titanium dioxide (TiO_2) has been the subject of extensive research in recent decades. Due to its equivalent energy gap, researchers have suggested Zinc oxide (ZnO) as an alternative for titanium dioxide (TiO_2) as a photocatalyst. However, ZnO exhibits a greater absorption efficiency across a wider range of the solar light spectrum than TiO_2.[7,8] The development of ZnO-based materials has progressed significantly as a result of improvements in synthesis and characterization techniques, as well as the discovery of novel uses in photonics, optics, electronics, sensors, piezoelectrics, and catalysts.[9]

Zinc-based semiconductors, recognized for their stability, broad band gap, and catalytic efficacy, are extensively utilized in electronics, sensors, solar cells, and photocatalysis. Their function in photocatalysis is essential, particularly as the textiles industry releases 15% of world dye production into aquatic environments, resulting in pollution.[10] ZnO generally crystallizes in the wurtzite form, making it the main focus of photocatalytic studies.[11] The synthesis of zinc oxide nanostructures is

School of Metallurgy and Materials Engineering, Iran University of Science and Technology (IUST), Tehran, Iran. E-mail: ashiri@iust.ac.ir

influenced by various strategies and the kinetics of the synthesis processes.[1] The shape of nanostructured materials, such as zero-dimensional (D0), one-dimensional (D1), two-dimensional (D2), and three-dimensional (D3) nanostructures, plays a crucial role in determining the photocatalytic activity of ZnO due to crystal growth in different morphologies.[12]

The process of degrading a pollutant through chemical reactions occurs on the surface of the photocatalyst. Consequently, the characteristics of the catalyst's surface have an important effect.[13] The synthesis methods significantly affect the crystallinity, shape, dimensional stability, particle size, and overall features of zinc oxide nanostructures.[14] Given that the properties of a material are influenced by the synthesis method, the selection of a preparation method is an important aspect in designing ZnO nanoparticles for specific uses.[15] The selection of synthesis method is dependent on the accessibility of the facilities, the expense, and the required catalyst properties.[16] Due to the variation in electron emission properties, optical properties, and electrical properties observed in different ZnO morphologies, extensive study has been conducted to identify the most effective fabrication process for achieving ZnO with exceptional properties.[17]

Typically, nanomaterials can be produced using physical, chemical, biological, mechanical or a combination of these techniques. Nanomaterials are produced by the chemical synthesis process by mixing materials in chemistry and fine-tuning the reaction parameters.[18] Various methods can be used to synthesize ZnO nanostructures, such as hydrothermal,[19,20] solvothermal,[14] sol–gel,[21,22] microemulsion,[23] sonochemical,[24] and solution combustion.[25] The sol–gel method is highly desirable for synthesizing ZnO nanostructures because of its cost-effectiveness, reliability, reproducibility, simplicity, low temperature requirements, precise control over physical properties and nanoparticle morphology, compositional homogeneity, and favorable optical properties.[8,26] The selection of solvent type in the synthesis process significantly influences the quality of the produced ZnO and the size of the nanoparticles.[27] The synthesis of zinc oxide is significantly influenced by selection of the solvent, which can influence the morphology,[28] particle size,[29] crystallinity,[30] and photocatalytic activity of the resulting material. In this study, we synthesized zinc oxide powder by sol–gel method and with different solvents to investigate the effect of solvent type on the morphology and photocatalytic properties of zinc oxide. Comparing the results of the current study with the results from prior researches, reveals that the main challenge in earlier studies was the long duration of MB dye degradation, while this study has achieved a very short degradation time. The results of this study indicate that the synthesized photocatalyst material exhibits remarkable photocatalytic performance, an obtainment which has not been documented in prior researches.

2. Experimental procedure

2.1. Materials

Zinc acetate dihydrate (Zn $(CH_3COO)_2{\cdot}2H_2O$), oxalic acid dihydrate $((COOH)_2{\cdot}2H_2O)$, ethanol (C_2H_6O), 1-Propanol (C_3H_8O) and 1,4-Butanediol ($C_4H_{10}O_2$) (99.9% pure) were purchased from Merck. All the reagents were used without any additional purification.

2.2. Synthesis of ZnO

To synthesis ZnO (see graphical flowchart of preparation in Fig. 1), a suitable amount of zinc acetate dihydrate was added to 50 mL of ethanol in pot 1.

The mixture was then stirred using a magnetic stirrer for 30 min at 50 °C. A measured amount of oxalic acid was added to 25 mL of ethanol in pot 2 and placed on a magnetic stirrer to dissolve at room temperature. Then, the contents of pot 2 were added to pot 1 until a viscous white solution was obtained. When zinc acetate dihydrate reacts with oxalic acid dihydrate in ethanol, zinc oxalate is formed according to the following reaction:[31]

$$Zn(CH_3CO_2)_2{\cdot}2H_2O + H_2C_2O_4{\cdot}2H_2O \rightarrow ZnC_2O_4 + 2CH_3CO_2H + 4H_2O \quad (R1)$$

The solution was stirred at a temperature of 70 °C using a magnetic stirrer until it transforms into a gel-like substance. The resulting gel was subsequently placed in an oven set at 80 °C to dry it overnight. The dried gel was calcined at a temperature of 600 °C for a period of 240 min. It appears that zinc oxalate is converted into zinc oxide nanoparticles *via* the following possible reaction:

$$ZnC_2O_4 \rightarrow ZnO + CO_2 + CO \quad (R2)$$

The zinc oxalate formed can be thermally decomposed to produce ZnO nanoparticles. Subsequently, the resulting powder was crushed using a mortar. Using 1-propanol and 1,4-butanediol solvents, the process of producing ZnO was repeated. The resulting powders from solvents ethanol, 1-propanol and 1,4-butanediol were designated as A1, A2, and A3, respectively.

2.3. Characterization

The phase and crystal structure of the synthesized powders were characterized using XRD analysis (Bourevestnik DRON-8 model). This analysis was performed using an accelerating voltage of 40 kV and Cu K_α radiation with a 1.54 Å wavelength. The step size and time per step for this analysis were selected as 0.04° and 0.5 s, respectively, and the analysis was performed over an angle range of 5 to 80 degrees. Scanning electron microscopy (SEM; Tescan MIRA3 model) was used to examine the microstructure of the samples. Meanwhile, the surface morphology and particle size of the resultant powder were characterized using the mentioned characterization methods. The identification of functional groups was carried out using the PerkinElmer FT-IR Spectrometer-Spectrum 100, which operated in the range of 4000 to 400 cm^{-1}, 4 cm^{-1} resolution and 0.2 cm s^{-1} scan speed using infrared spectrometry. To perform this analysis, the samples were prepared as KBr pellets. Three spectra were recorded for each sample. The photoluminescence (PL) spectra of the synthesized samples were recorded using the Varian Cary Eclipse equipment at an excitation wavelength of 320 nm and in the wavelength range of 300–600 nm. UV-visible spectroscopy was conducted in a solid sample to examine the

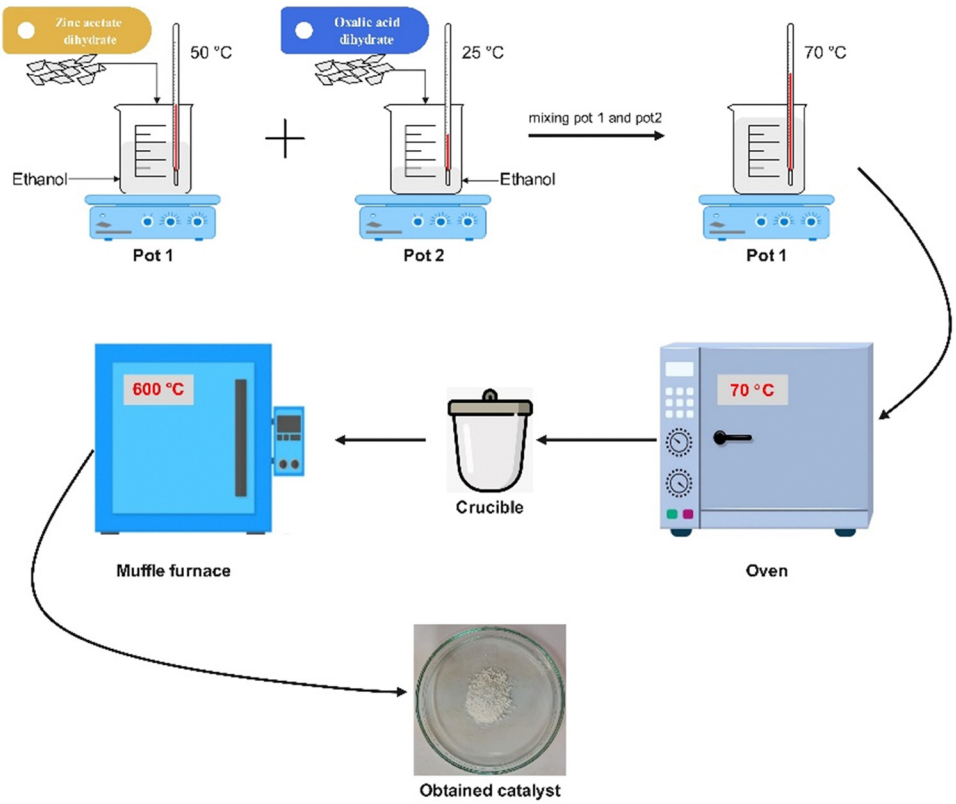

Fig. 1 Schematic of synthesizing process of ZnO photocatalyst.

optical characteristics of the powders obtained and to estimate the band gap of the synthesized materials using a Shimadzu 2550 spectrophotometer.

2.4. Photocatalytic activity test

To determine the photocatalytic activity of the obtained powder, the degradation of MB dye was examined using ultraviolet light. To achieve this objective, a solution of MB dye (100 mL) with a concentration of 5 mg L^{-1} was exposed to UV irradiation in the presence of 0.1 g of each of the synthesized ZnO powders. In order to carry out the UV light examination, sample was placed in equipment that included a magnetic stirrer for stirring the mixture and two Philips TL 8 W BLB lamps located 15 cm far from the sample and emitting ultraviolet light with a wavelength in the range of 360 nm to 380 nm. Initially, the sample was placed in the device for 60 min without turning on the lamps to achieve absorption-desorption equilibrium, and then the ultraviolet lamps were turned on to irradiate the sample, while samples were collected at 10-min intervals. The concentration of degraded solutions was determined by analyzing them using the BRAIC UV-2100 Double Beam UV-Vis spectrophotometer using two rounds of centrifugation at 4000 rpm for 200 min.

3. Results and discussions

Fig. 2 shows the XRD patterns of the powders that were synthesized in the current work. The figure clearly shows that

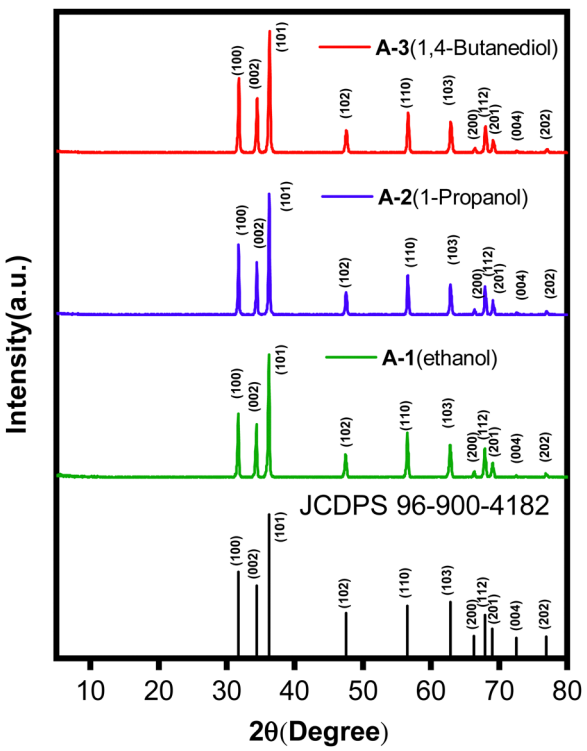

Fig. 2 XRD pattern of ZnO sample synthesized by sol–gel method.

the peaks at 2θ of 31.70°, 34.37°, 36.17°, 47.45°, 56.52°, 62.77°, 66.30°, 67.87°, 69.02°, 72.52°, and 76.87° in the sample synthesized by ethanol solvent (A1) correspond to the crystal planes (100), (002), (101), (102), (110), (103), (200), (112), (201), (004), and (202), respectively, given by JCPDS card number 96-900-4182. These characteristics are also seen in samples synthesized with 1-propanol (A2) and 1,4-butanediol (A3), providing evidence that the synthesized powders consist of single phase hexagonal wurtzite ZnO. Furthermore, no extra peaks are seen in these patterns indicating the absence of impurities, by-products, and unwanted phase formation. It can also be concluded that changing the type of solvent in the synthesis of zinc oxide does not affect the formation of by-product and unwanted phase.

By applying Scherer's equation and determining the full width at half maximum (FWHM) for each peak in the samples, it is possible to calculate the average size of the crystallites for each sample. The Scherer's equation is defined as follows:[32]

$$D = \frac{K\lambda}{\beta \cos\theta} \quad (1)$$

where D indicates the size of the crystallite, K is Scherer's constant, λ is the X-ray wavelength, and θ represents the FWHM value. Table 1 shows the crystallite and particle size for the synthesized samples. It is evident that sample A2 has the largest crystallite size, while sample A3 has the smallest one. The solvent type significantly influenced ZnO crystallite size. In a study conducted by Ludmila Motelica *et al.*[33] on the effect of solvent type on the synthesis and photocatalytic properties of ZnO, it was found that the crystallite size changes with variation of the solvent type. It is important to note that when the size of the crystallites decreases, the surface area and surface defects increase. This causes the charge carriers to separate and inhibit their recombination by trapping them.[34] Consequently, the photocatalytic activity is enhanced. Among the examined samples, sample A1 has the optimal crystallite size and demonstrates better photocatalytic performance compared to the other samples.

Table 1 The crystallite size, particle size and band gap of samples

Sample name	Crystallite size (nm)	Particle size (nm)	Band gap (eV)
A1	45.5	161	3.18
A2	47.7	163	3.17
A3	37.5	61	3.20

The selection of solvent can affect particle morphology and size. Ludmila Motelica *et al.*[35] synthesized zinc oxide by the solvothermal method using three different solvents and discovered that the change of the solvent during synthesis influences the morphology and particle size. They found that ZnO obtained from each solvent exhibits different morphology and particle size; samples synthesized with *n*-butanol, ethylene glycol and glycerin exhibited polyhedral, round, and hexagonal polycrystalline morphologies and 27 nm, 44 nm and 120 nm particle sizes, respectively.

Fig. 3 shows scanning electron microscopy images of ZnO powders synthesized *via* the sol–gel method. These images were taken at different magnifications. In the FE-SEM images, it is observed that with the change of solvent, slight changes in morphology occur. Sample A1, which was synthesized with ethanol, has semi-spherical particles,[2] and the porosities are visible on surface of the sample. The particles are nearly spherical with an average particle size of 161 nm. In contrast, sample A2, synthesized with 1-propanol, has an average particle size of 163 nm and fewer spherical particles compared to sample A1. It also has sharp edges, and that type of porosity observed in sample A1 is not seen in sample A2. In sample A3

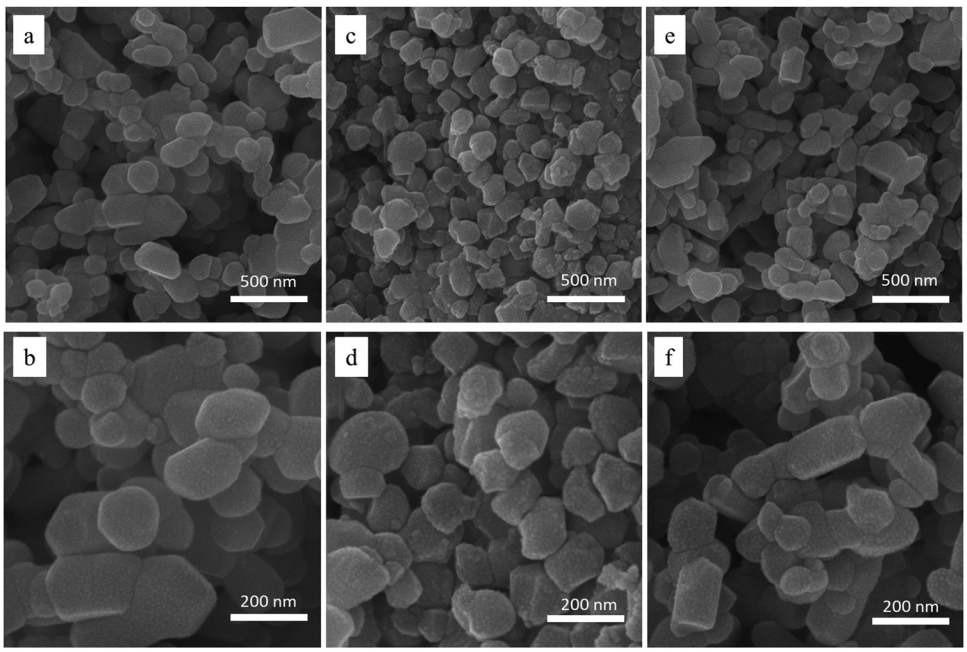

Fig. 3 FE-SEM images of (a) and (b) A1, (c) and (d) A2, (e) and (f) A3 sample.

that was synthesized by 1,4-butanediol, the pseudo-spherical particles that were seen in sample A1 are not seen here, and the particles have elongated morphology with an average particle size of 63 nm. This morphology in the samples is related to the presence of oxalic acid in the synthesis stage; oxalic acid as a passivating agent creates a uniform surface charge on the particles, which in turn creates an electrostatic barrier that prevents the agglomeration of particles.[36]

To investigate the characteristics of the atomic bonds and their related vibration modes,[37] Fourier transform infrared (FTIR) analysis was conducted on the ZnO sample, covering a spectral range of 4000 cm^{-1} to 400 cm^{-1}. Fig. 4 shows the infrared spectrum of the synthesized ZnO sample. The presence of distinct absorption peaks at 3440 cm^{-1} and 1630 cm^{-1} correspond to –OH functional groups and –O stretching vibration, respectively.[38] These vibrations are caused by the presence of absorbed moisture on the surface of powders. The activity of the photocatalyst in the photocatalysis process is determined by the quantity of functional groups formed on its surface. This is because OH– groups are able to transfer electrons to the photogenerated holes, leading to the generation of •OH radicals.[39] The peak observed at 1650 cm^{-1} corresponds to either the alcohol or moisture content. The presence of two peaks at 500 cm^{-1} and 530 cm^{-1} is assigned to stretching vibration of Zn–O bond.[40]

Fig. 5 shows the UV-vis absorption spectra of the samples synthesized in this work. It is observed that changing the solvent did not cause any shift in the absorption region, and all samples absorb light in the ultraviolet region, which is at a wavelength of around 374 nm. This peak can be attributed to the intrinsic band transition of ZnO.[41] Furthermore, it is evident that changing the solvent type in the synthesis process method does not result in any notable red shift[10] in the A1, A2, and A3 samples. The Kubelka–Munk equation[42] was used to calculate the band gap energy as follows:

$$(\alpha h\nu)^2 = A(h\nu - E_g) \quad (2)$$

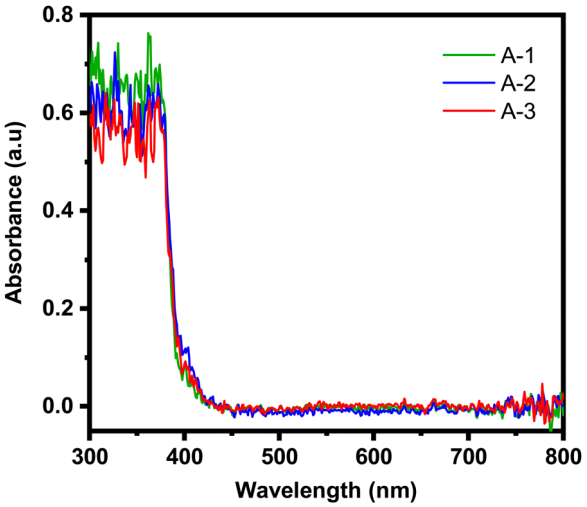

Fig. 5 UV-vis absorption spectra of the A1, A2 and A3 samples.

In this equation, α represents the absorption coefficient, $h\nu$ denotes the photon energy, A is the constant in the equation, and E_g is the band gap energy. The band gap energy values of samples were calculated using linear extrapolation of the Tauc plot, where $(\alpha h\nu)^2$ is plotted *versus* $h\nu$.[10] The Fig. 6 clearly demonstrates that all of the samples have almost the same band gap energy of approximately 3.2 eV; the band gap values were calculated to be 3.18 eV, 3.17 eV, and 3.20 eV for samples A1, A2, and A3, respectively (Table 1). The morphology of ZnO directly affects its band gap because changing in the particle size and changing the crystallite size can increase or decrease the band gap. ZnO nanostructures exhibit different optical and electronic behavior due to quantum effects and changes in the density of electronic states.[43,44] As shown in Table 1, the particle size and crystallite size did not change significantly, so the band gap size in the samples change slightly.

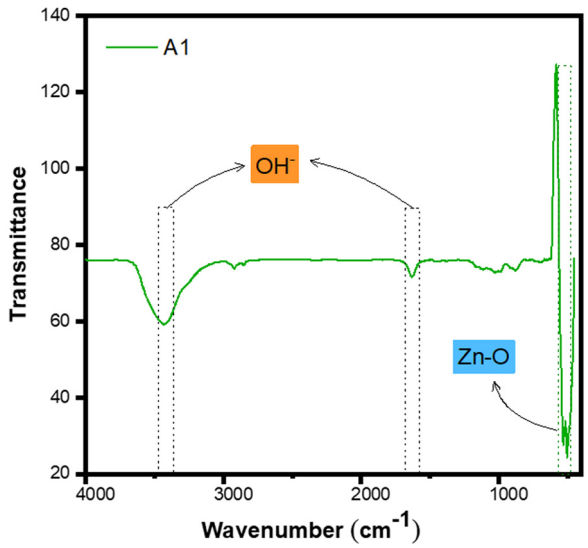

Fig. 4 FTIR spectrum of the A1 sample.

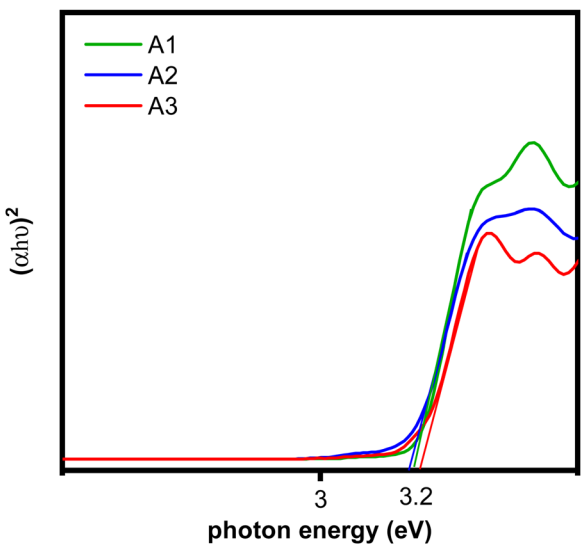

Fig. 6 Tauc plot of A1, A2 and A3 samples.

Photoluminescence (PL) analysis is an appropriate and efficient technique to examine the recombination and trapping of charge carriers in semiconductor materials.[45] The variations in intensity of PL across the samples can be explained by the impact of various solvents utilized during the synthesis process. The selection of solvent may significantly impact the crystallinity,[38] surface defects,[39] and particle size[40] of the resultant material, all of which are critical to charge carrier separation and photocatalytic activity.[41] Fig. 7 displays the photoluminescence spectra of A1, A2, and A3 samples. Only one strong peak at a wavelength of around 400 nm is observed in all samples. This peak corresponds to the near band-edge (NBE) exciton emission, which is characterized by the recombination of free excitons resulting from an excitation–excitation collision process.[46,47] Fig. 7 clearly demonstrates that sample A3 exhibits the highest intensity, whereas sample A2 displays the lowest intensity, which aligns with the results of the photocatalytic test.

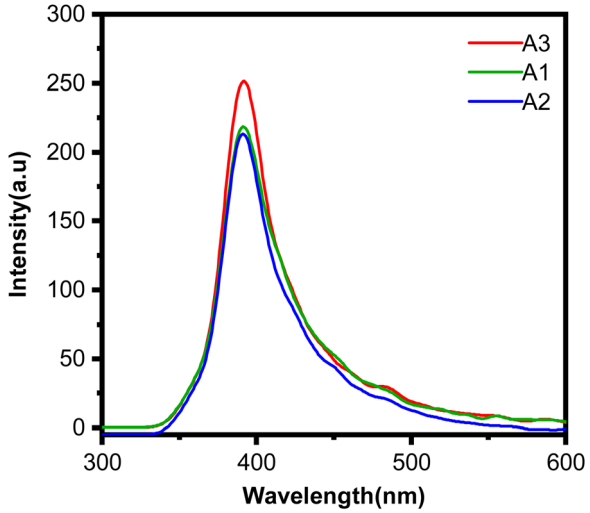

Fig. 7 PL analysis of A1, A2 and A3 samples.

Fig. 8 displays the UV-vis spectra of a 5 ppm concentration MB dye solution at pH 9, after being exposed to ultraviolet light for various time intervals. The study conducted by Bhapkar *et al.*[48] showed that pH 9 provides the most optimal photocatalytic activity for ZnO. The main absorption peak of MB dye appears at a wavelength of 663 nm. It is evident that the intensity of this peak has decreased over time as a result of photocatalytic activity and the reduction in the concentration of MB dye in the solution. Furthermore, Fig. 9a displays the results of photodegradation of the MB dye following a duration of 40 min. Sample A1 exhibits the highest degradation rate of 98%, while sample A3 demonstrates the lowest degradation rate of 95%. These findings align with the

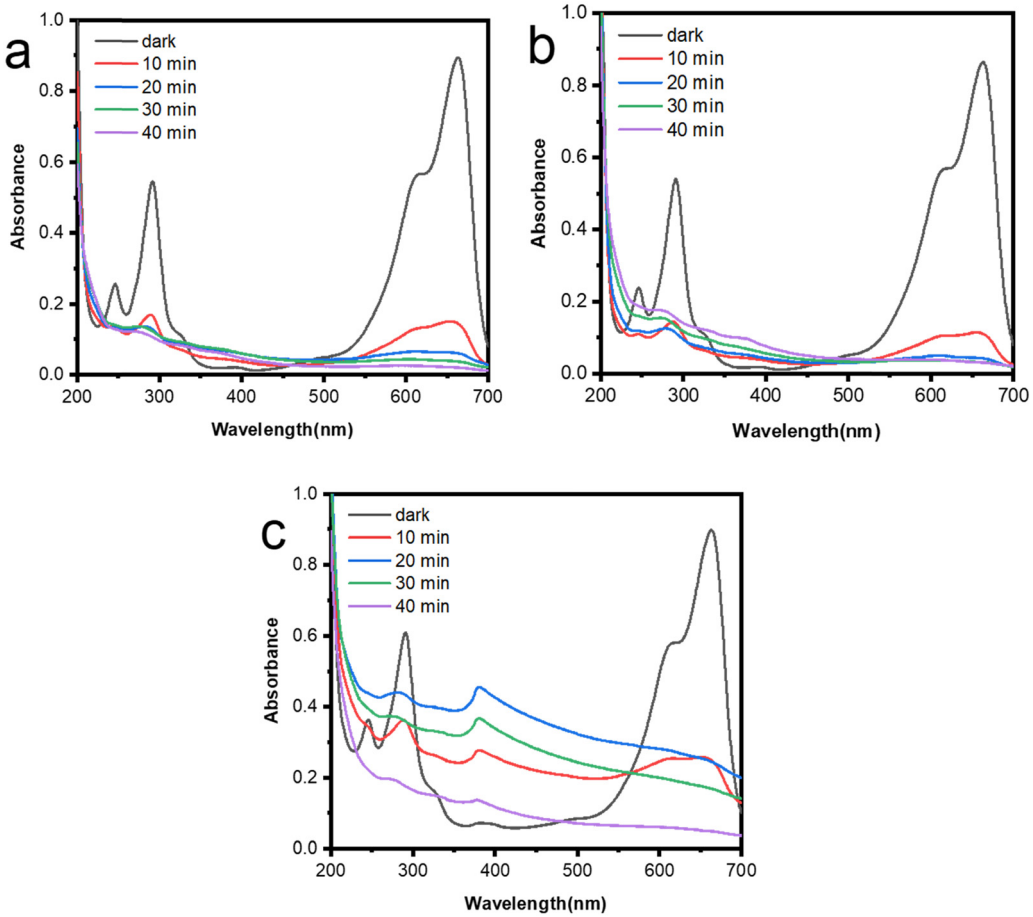

Fig. 8 UV-vis spectra of MB dye during photodegradation in presence of (a) A1 (b) A2 (c) A3 photocatalysts.

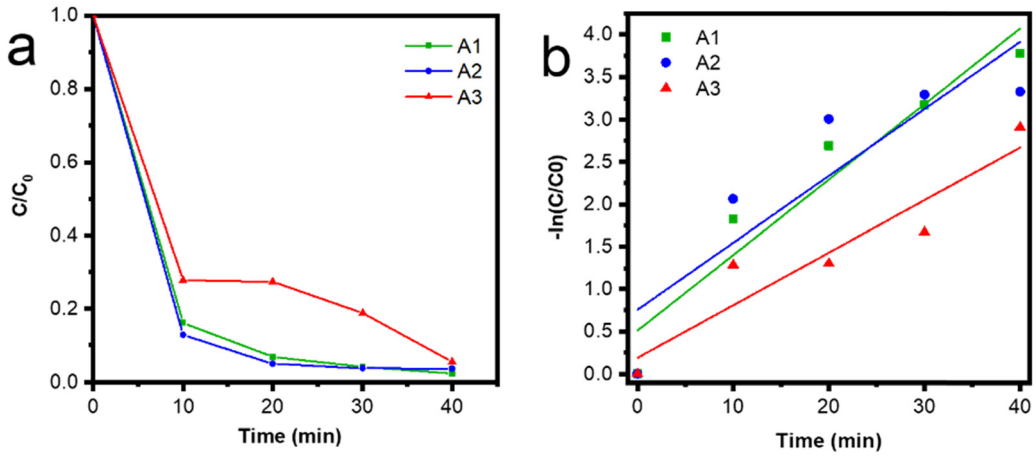

Fig. 9 (a) Photodegradation efficiency of samples and (b) first-order kinetics of MB dye in 40 min under irradiation of UV light.

results acquired in the preceding stages. As shown in Fig. 9b, the rate constant for the degradation of MB dye through photodegradation can be calculated by utilizing the modified Langmuir- Hinshelwood equation, which is based on first-order reaction kinetics[49] as follows:

$$\ln\left(\frac{C_{eq}}{C_0}\right) = -kt \quad (3)$$

where C and C_{eq} are the final and equilibrium concentrations of MB dye, respectively, and k represents the reaction rate constant. The values of K and linear correlation coefficients (R^2) are shown in Table 2, showing that sample A1 has a higher degradation rate and good agreement with the first-order kinetic equation than the other samples. The equilibrium concentration of MB dye solution compared to the dye concentration after 40 min of UV light irradiation in the presence of each of the catalysts is shown in Fig. 10 indicates high activity of the catalysts developed in this work.

In Table 2, the photocatalytic properties of the present work are compared with a number of similar works, and as shown in Table 2, the catalysts synthesized in this work show a significantly higher photocatalytic activity than other studies and have a much higher degradation rate. Due to the rapid degradation, the efficiency of this catalyst was compared with other studies in 10 min, and the results are presented in Table 2.

To examine the reusability and stability of ZnO photocatalysts in the degradation of MB dye under UV irradiation, recycling studies have been conducted on samples A1, A2, and A3 during five consecutive cycles. The samples were collected after each cycle using centrifugation, subsequently washed with distilled water and ethanol, dried in an oven at 80 °C, and then reused for subsequent cycles. The results showed that the MB dye removal

Table 2 Photocatalytic activity of ZnO photocatalyst obtained in this study compared to similar published studies

Sample name	K (min^{-1})	Linear regression coefficient (R^2)	Photocatalytic efficiency after 10 min irradiation (%)	Photocatalytic efficiency (%)	MB dye concentration (ppm)	Exposure time (min)	Light source	Catalyst dosage (g L^{-1})	Synthesis route	Ref.
A1	0.089	0.920	84	98	5	40	UV	1	Sol–gel	This work
A2	0.078	0.789	87	97	5	40	UV	1	Sol–gel	This work
A3	0.061	0.889	73	95	5	40	UV	1	Sol–gel	This work
ZnO	0.013	0.991	20	95.3	10	70	Sunlight	0.25	Microwave assisted	50
ZnO	0.010	0.982	20	92	10	180	UV	1	Sol–gel	51
ZnO	0.048	—	30	93	3	60	Visible	0.2	Wet chemical	52
$Zn_{0.88}Ni_{0.12}O$	0.0810		50	98						
ZnO	—	—	—	58	12	120	UV	2	Sol–gel	53
$Fe_{0.8}$–ZnO				93						
ZnO	—	—	15	65	1	50	Solar light	0.5	Hydrothermal	54
ZnO	0.022		20	92	15	120	UV	1	Biosynthesis	55
ZnO	—	—	10	82	15	180	UV	1	Solution combustion	25
ZnO	—	—	22	98	15	180	UV	1	Solution combustion	56
ZnO	0.015	0.985	50	86	5	90	Visible	1.6	Co-precipitation	57
TiO_2	0.006	—	—	92	10	360	Sunlight	0.03	Sol–gel	58
P-doped TiO_2	0.017	—	—	97	5	180	Visible	3	Precipitation	59
Bio-TiO_2	0.0197	—	—	79	37	60	UV	0.6	Biosynthesis	60
CuO/rGO	0.0208	—	—	92	20	90	Solar light	0.5	Sol–gel	61
Flower-like CuO–ZnO	0.099	0.989		98	100	30	Sunlight	0.5	Hydrothermal	62
α-Fe_2O_3: ZnO	0.036	0.992	—	99	30	120	Solar light	0.4	Chemical precipitation	63

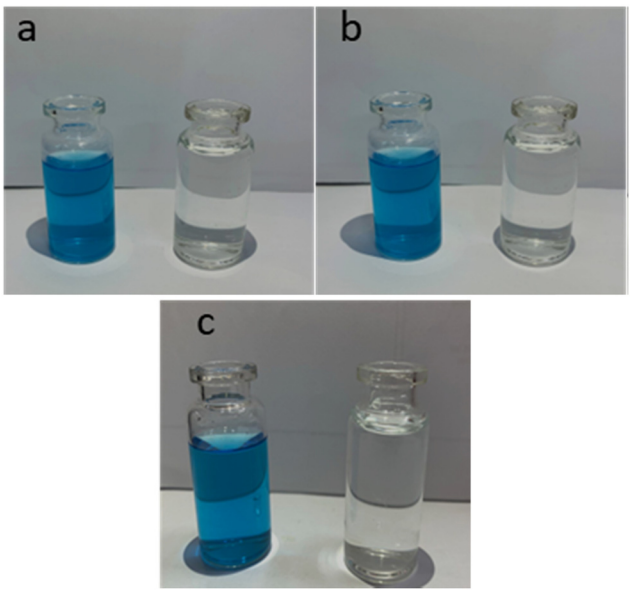

Fig. 10 Degradation of MB dye after 40 min UV light irradiation in presence of (a) A1, (b) A2 and (c) A3 photocatalysts.

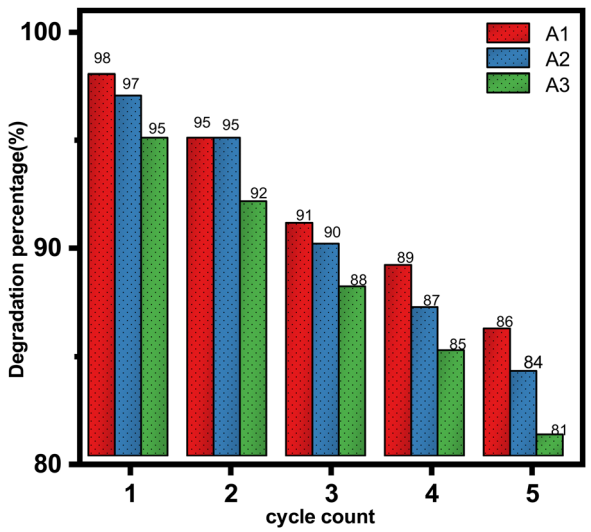

Fig. 11 Cyclic stability and reusability of the photocatalyst for A1, A2, and A3 samples in five cycles.

efficiency (Fig. 11) for samples A1, A2, and A3 decreased from 98%, 97%, and 95% to 86%, 84%, and 83%, respectively, throughout five cycles. This slight decrease in photocatalytic performance was due to the partial loss of photocatalyst during repeated cycles, which indicates the high stability of this photocatalyst in MB dye degradation processes under UV light irradiation.

The radical scavenger test was carried out to identify the reactive species involved in the photocatalytic process for the degradation of MB dye, and the results are shown in Fig. 12. This study investigated the impact of EDTA, IPA and $AgNO_3$ on the dye degradation process under UV irradiation and 1 mM of each radical scavenger was employed, with an initial dye concentration of 5 ppm and a photocatalyst dosage of 1 g L^{-1}. The

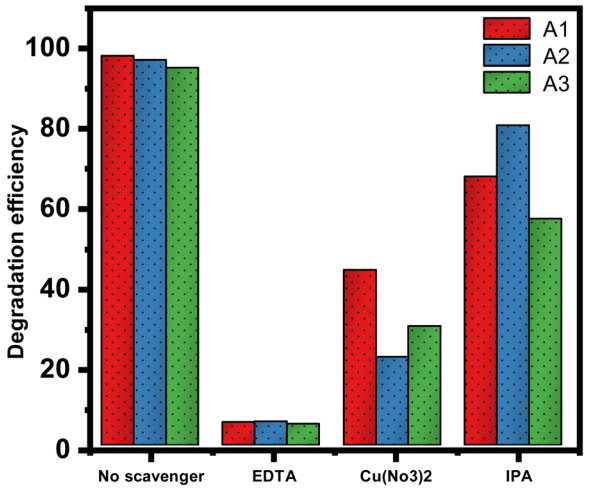

Fig. 12 Degradation efficiency of A1, A2, and A3 samples in presence of various scavengers.

samples were subjected to UV irradiation for 40 min, using A1, A2, and A3 as the photocatalysts, and the dye degradation efficiency was evaluated in the presence of each scavenger.

As shown in Fig. 11, the test results revealed that sample A1 exhibited a dye degradation efficiency of 98% without a scavenger presence. Following the incorporation of EDTA, IPA and $AgNO_3$, the values reduced to 5.69%, 44.09%, and 67.63%, respectively. In sample A2, the dye degradation efficiency without a scavenger was 97%, which diminished to 5.88%, 22.13%, and 80.43% in the presence of EDTA, IPA, and $AgNO_3$, respectively. In sample A3, the dye degradation efficiency without a scavenger was 95%, which decreased to 5.35%, 29.95%, and 57.04% with introducing the EDTA, IPA, and $AgNO_3$, respectively.

The results demonstrate that the presence of EDTA results in the most significant decrease in dye degradation in all samples, underscoring its potent capacity to suppress reactive oxygen species (ROS) by functioning as a hole (h^+) scavenger.[64] IPA, which predominantly scavenges hydroxyl ($^\bullet OH$) radicals,[2] exhibited a moderate impact on dye degradation reduction. On the other hand, $AgNO_3$, known to be an electron (e^-) scavenger,[65] showed distinct impacts depending on the material. In sample A2, $AgNO_3$ demonstrated a diminished effect on dye degradation, maintaining a degradation efficiency of 80.43%. The use of EDTA significantly reduced dye degradation efficiency (to approximately 5% across all samples), indicating its importance as a hole scavenger through the adsorption of ROS. This significant reduction indicates that holes (h^+) are the main factors to the photocatalytic degradation process.

According to the experimental data obtained in this study, the mechanism illustrated in Fig. 13 may be proposed for the degradation of MB dye. Therefore, after UV light irradiation, electrons and holes situated in the conduction band (CB) and valence band (VB), respectively due to the degradation of methylene blue dye. The electrons photogenerated in the conduction band react with oxygen to produce O_2^- radicals. The holes in VB interact with water resulting in the formation of $^\bullet OH$ radicals. These radicals interact with the dye resulting in its decomposition.

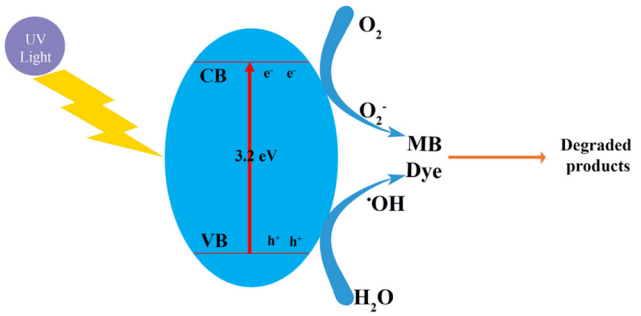

Fig. 13 Possible degradation mechanism of MB dye by zinc oxide photocatalyst under visible light irradiation.

4. Conclusions

In this study, zinc oxide (ZnO) nanoparticles were synthesized using a sol–gel method and three different solvents (ethanol, 1-propanol, and 1,4-butanediol) to investigate the effect of the solvent type on the structural, morphological, and photocatalytic properties. X-ray diffraction (XRD) patterns showed that all samples exhibited a hexagonal wurtzite structure, with differences in crystallite size dependent on the type of solvent used. Scanning electron microscopy (SEM) photos verified that the morphology and size distribution of the particles were influenced by the type of solvent. FTIR spectroscopy results confirmed the presence of –OH functional groups, which are important for photocatalytic activity. UV-vis spectroscopy showed that all samples indicated a comparable energy gap, ranging from around 3.17 to 3.20 eV. Photoluminescence (PL) spectroscopy revealed that the fluorescence emission intensity differed among samples, with the sample exhibiting the lowest crystal size (synthesized by 1,4-butanediol) demonstrating the highest emission intensity suggesting accelerated recombination of charge carriers. The photocatalytic degradation of methylene blue under UV irradiation demonstrated that the sample synthesized using ethanol had the most effective photocatalytic activity, achieving a degradation of 98% of the dye within 40 minutes. Finally, the results of this study demonstrated that the properties of ZnO nanoparticles are significantly influenced by the type of solvent. The optimization of the structural characteristics and photocatalytic performance of this material can be assisted by the selection of an appropriate solvent.

Data availability

The data will be available on request.

Conflicts of interest

There are no conflicts to declare.

References

1 F. Abdullah, N. A. Bakar and M. A. Bakar, Current advancements on the fabrication, modification, and industrial application of zinc oxide as photocatalyst in the removal of organic and inorganic contaminants in aquatic systems, *J. Hazard. Mater.*, 2022, **424**, 127416.
2 K. Pompapathi, *et al.*, Visible-light-driven mentha spicata L.-mediated Ag-doped $Bi_2Zr_2O_7$ nanocomposite for enhanced degradation of organic pollutants, electrochemical sensing, and antibacterial applications, *ACS Environ. Au*, 2024, **4**(2), 106–125.
3 P. Karuppasamy, S. Senthilkumar, O. Ganeshbabu, S. Pitchaimuthu, M. Sennappan and V. Rajapandian, Sonochemical synthesis and characterization of visible light driven CuO@ g-C_3N_4 nano-photocatalyst for eriochrome black T dye degradation in industrial dye effluent, *Russ. J. Inorg. Chem.*, 2022, **67**(13), 2153–2165.
4 S. G. Kumar and R. Kavitha, Lanthanide ions doped ZnO based photocatalysts, *Sep. Purif. Technol.*, 2021, **274**, 118853.
5 A. Zaleska-Medynska, *Metal oxide-based photocatalysis: fundamentals and prospects for application*, Elsevier, 2018.
6 S. G. Kumar and K. K. Rao, Zinc oxide based photocatalysis: tailoring surface-bulk structure and related interfacial charge carrier dynamics for better environmental applications, *RSC Adv.*, 2015, **5**(5), 3306–3351.
7 S. Goktas and A. Goktas, A comparative study on recent progress in efficient ZnO based nanocomposite and heterojunction photocatalysts: A review, *J. Alloys Compd.*, 2021, **863**, 158734.
8 C. B. Ong, L. Y. Ng and A. W. Mohammad, A review of ZnO nanoparticles as solar photocatalysts: Synthesis, mechanisms and applications, *Renewable Sustainable Energy Rev.*, 2018, **81**, 536–551.
9 J. van Embden, S. Gross, K. R. Kittilstved and E. Della Gaspera, Colloidal approaches to zinc oxide nanocrystals, *Chem. Rev.*, 2022, **123**(1), 271–326.
10 P. Karuppasamy, N. R. N. Nisha, A. Pugazhendhi, S. Kandasamy and S. Pitchaimuthu, An investigation of transition metal doped TiO_2 photocatalysts for the enhanced photocatalytic decoloration of methylene blue dye under visible light irradiation, *J. Environ. Chem. Eng.*, 2021, **9**(4), 105254.
11 M. Samadi, M. Zirak, A. Naseri, M. Kheirabadi, M. Ebrahimi and A. Z. Moshfegh, Design and tailoring of one-dimensional ZnO nanomaterials for photocatalytic degradation of organic dyes: a review, *Res. Chem. Intermed.*, 2019, **45**, 2197–2254.
12 A. Hezam, *et al.*, Strategies to enhance ZnO photocatalyst's performance for water treatment: a comprehensive review, *Chem. Rec.*, 2022, **22**(7), e202100299.
13 P. P. Vhangutte, *et al.*, Influence of synthesis methods on physical and photocatalytic properties of Bi2WO6 for decomposition of organic dyes and Cr (VI) reduction, *Bull. Mater. Sci.*, 2023, **46**(2), 56.
14 M. T. Noman, N. Amor and M. Petru, Synthesis and applications of ZnO nanostructures (ZONSs): A review, *Crit. Rev. Solid State Mater. Sci.*, 2022, **47**(2), 99–141.
15 A. Król, P. Pomastowski, K. Rafińska, V. Railean-Plugaru and B. Buszewski, Zinc oxide nanoparticles: Synthesis, antiseptic activity and toxicity mechanism, *Adv. Colloid Interface Sci.*, 2017, **249**, 37–52.

16 I. Medina-Ramírez, A. Hernández-Ramírez and M. L. Maya-Trevino, Synthesis methods for photocatalytic materials, *Photocatalytic Semiconductors: Synthesis, Characterization, and Environmental Applications*, 2015, pp. 69–102.
17 M. Rezapour and N. Talebian, Comparison of structural, optical properties and photocatalytic activity of ZnO with different morphologies: Effect of synthesis methods and reaction media, *Mater. Chem. Phys.*, 2011, **129**(1–2), 249–255.
18 G. K. Weldegebrieal, Synthesis method, antibacterial and photocatalytic activity of ZnO nanoparticles for azo dyes in wastewater treatment: A review, *Inorg. Chem. Commun.*, 2020, **120**, 108140.
19 I. Ahmad, *et al.*, Recent progress in rare earth oxides and carbonaceous materials modified ZnO heterogeneous photocatalysts for environmental and energy applications, *J. Environ. Chem. Eng.*, 2022, **10**(3), 107762.
20 T. Chankhanittha and S. Nanan, Hydrothermal synthesis, characterization and enhanced photocatalytic performance of ZnO toward degradation of organic azo dye, *Mater. Lett.*, 2018, **226**, 79–82.
21 R. Mahdavi and S. S. A. Talesh, Sol-gel synthesis, structural and enhanced photocatalytic performance of Al doped ZnO nanoparticles, *Adv. Powder Technol.*, 2017, **28**(5), 1418–1425.
22 R. Mahdavi and S. S. A. Talesh, The effect of ultrasonic irradiation on the structure, morphology and photocatalytic performance of ZnO nanoparticles by sol-gel method, *Ultrason. Sonochem.*, 2017, **39**, 504–510.
23 P. Falak, S. Hassanzadeh-Tabrizi and A. Saffar-Teluri, Synthesis, characterization, and magnetic properties of ZnO-ZnFe2O4 nanoparticles with high photocatalytic activity, *J. Magn. Magn. Mater.*, 2017, **441**, 98–104.
24 S. Shenoy, S. Ahmed, I. M. Lo, S. Singh and K. Sridharan, Rapid sonochemical synthesis of copper doped ZnO grafted on graphene as a multi-component hierarchically structured visible-light-driven photocatalyst, *Mater. Res. Bull.*, 2021, **140**, 111290.
25 Z. K. Bolaghi, S. Masoudpanah and M. Hasheminiasari, Photocatalytic activity of ZnO/RGO composite synthesized by one-pot solution combustion method, *Mater. Res. Bull.*, 2019, **115**, 191–195.
26 M. Parashar, V. K. Shukla and R. Singh, Metal oxides nanoparticles via sol–gel method: a review on synthesis, characterization and applications, *J. Mater. Sci.: Mater. Electron.*, 2020, **31**, 3729–3749.
27 K. Kanade, B. Kale, R. Aiyer and B. Das, Effect of solvents on the synthesis of nano-size zinc oxide and its properties, *Mater. Res. Bull.*, 2006, **41**(3), 590–600.
28 D. K. Yavuz, M. El Accen and M. Bedir, Unlocking the potential of ZnO nanorods: Structural insights for enhanced photocatalytic activity, *J. Phys. Chem. Solids*, 2024, **193**, 112120.
29 M. Montero-Muñoz, *et al.*, Role of defects on the enhancement of the photocatalytic response of ZnO nanostructures, *Appl. Surf. Sci.*, 2018, **448**, 646–654.
30 M. Montero-Muñoz, J. Ramos-Ibarra, J. Rodríguez-Páez, A. Ramirez and J. Huamaní-Coaquira, Shape-control of Zinc Oxide nanoparticles: enhancing photocatalytic activity under UV irradiation, *J. Phys.: Conf. Ser.*, 2017, **792**(1), 012068.
31 Z. Y. Shnain, *et al.*, The effect of solvent-modification on the physicochemical properties of ZnO nanoparticles synthesized by sol-gel method, *Bull. Chem. React. Eng. Catal.*, 2022, **17**(1), 46–52.
32 A. Patterson, The Scherrer formula for X-ray particle size determination, *Phys. Rev.*, 1939, **56**(10), 978.
33 L. Motelica, *et al.*, Influence of the alcohols on the zno synthesis and its properties: The photocatalytic and antimicrobial activities, *Pharmaceutics*, 2022, **14**(12), 2842.
34 I. Okeke, *et al.*, Impact of particle size and surface defects on antibacterial and photocatalytic activities of undoped and Mg-doped ZnO nanoparticles, biosynthesized using one-step simple process, *Vacuum*, 2021, **187**, 110110.
35 L. Motelica, *et al.*, Antibacterial activity of solvothermal obtained ZnO nanoparticles with different morphology and photocatalytic activity against a dye mixture: methylene blue, rhodamine B and methyl orange, *Int. J. Mol. Sci.*, 2023, **24**(6), 5677.
36 A. Stanković, L. Veselinović, S. Škapin, S. Marković and D. Uskoković, Controlled mechanochemically assisted synthesis of ZnO nanopowders in the presence of oxalic acid, *J. Mater. Sci.*, 2011, **46**, 3716–3724.
37 S. Ahmad, *et al.*, Sol-gel synthesis of nanostructured ZnO/SrZnO2 with boosted antibacterial and photocatalytic activity, *Ceram. Int.*, 2022, **48**(2), 2394–2405.
38 J. Li, *et al.*, MXene Ti3C2 decorated g-C3N4/ZnO photocatalysts with improved photocatalytic performance for CO2 reduction, *Nano Mater. Sci.*, 2023, **5**(2), 237–245.
39 M. Ahmad, *et al.*, Preparation of highly efficient Al-doped ZnO photocatalyst by combustion synthesis, *Curr. Appl. Phys.*, 2013, **13**(4), 697–704.
40 P. Hemnil, Y. Prapawasit, V. Karthikeyan, T. Wongwuttanasatian and V. Seithtanabutara, Novel cubic heterojunction Fe_2O_3/ZnO composite for the photocatalyst application, *Mater. Today: Proc.*, 2023, **75**, 1–8.
41 I. Ahmad, Comparative study of metal (Al, Mg, Ni, Cu and Ag) doped ZnO/g-C3N4 composites: efficient photocatalysts for the degradation of organic pollutants, *Sep. Purif. Technol.*, 2020, **251**, 117372.
42 Ł. Haryński, A. Olejnik, K. Grochowska and K. Siuzdak, A facile method for Tauc exponent and corresponding electronic transitions determination in semiconductors directly from UV–Vis spectroscopy data, *Opt. Mater.*, 2022, **127**, 112205.
43 R. Marotti, P. Giorgi, G. Machado and E. Dalchiele, Crystallite size dependence of band gap energy for electrodeposited ZnO grown at different temperatures, *Sol. Energy Mater. Sol. Cells*, 2006, **90**(15), 2356–2361.
44 K. M. Lee, C. W. Lai, K. S. Ngai and J. C. Juan, Recent developments of zinc oxide based photocatalyst in water treatment technology: a review, *Water Res.*, 2016, **88**, 428–448.
45 I. N. Reddy, *et al.*, Excellent visible-light driven photocatalyst of (Al, Ni) co-doped ZnO structures for organic dye degradation, *Catal. Today*, 2020, **340**, 277–285.
46 N. D. Dien, P. T. T. Ha, X. H. Vu, T. T. Trang, T. D. T. Giang and N. T. Dung, Developing efficient CuO nanoplate/ZnO

nanoparticle hybrid photocatalysts for methylene blue degradation under visible light, *RSC Adv.*, 2023, **13**(35), 24505–24518.

47 V. Kumar, *et al.*, Origin of the red emission in zinc oxide nanophosphors, *Mater. Lett.*, 2013, **101**, 57–60.

48 A. Bhapkar, R. Prasad, D. Jaspal, M. Shirolkar, K. Gheisari and S. Bhame, Visible light driven photocatalytic degradation of methylene blue by ZnO nanostructures synthesized by glycine nitrate auto combustion route, *Inorg. Chem. Commun.*, 2023, **148**, 110311.

49 R. Mahdavi and S. S. Ashraf Talesh, The crystal structures, morphological, kinetics and photocatalytic activity studies of Al/Ca co-doped ZnO nanoparticles via the sol–gel process, *Int. J. Environ. Anal. Chem.*, 2022, **102**(18), 6684–6698.

50 R. Perez-Cuapio, J. A. Alvarado, H. Juarez and H. Sue, Sun irradiated high efficient photocatalyst ZnO nanoparticles obtained by assisted microwave irradiation, *J. Mater. Sci. Eng. B*, 2023, **289**, 116263.

51 K. A. Isai and V. S. Shrivastava, Photocatalytic degradation of methylene blue using ZnO and 2% Fe–ZnO semiconductor nanomaterials synthesized by sol–gel method: a comparative study, *SN Appl. Sci.*, 2019, **1**, 1–11.

52 I. Ahmad, *et al.*, ZnO and Ni-doped ZnO photocatalysts: Synthesis, characterization and improved visible light driven photocatalytic degradation of methylene blue, *Inorg. Chim. Acta*, 2022, **543**, 121167.

53 H. Khan, M. Habib, A. Khan and D. C. Boffito, A modified sol-gel synthesis to yield a stable Fe3 +/ZnO photocatalyst: Degradation of water pollutants and mechanistic insights under UV and visible light, *J. Environ. Chem. Eng.*, 2020, **8**(5), 104282.

54 N. Roy and S. Chakraborty, ZnO as photocatalyst: An approach to waste water treatment, *Mater. Today: Proc.*, 2021, **46**, 6399–6403.

55 C. Soto-Robles, *et al.*, Biosynthesis, characterization and photocatalytic activity of ZnO nanoparticles using extracts of Justicia spicigera for the degradation of methylene blue, *J. Mol. Struct.*, 2021, **1225**, 129101.

56 H. V. Vasei, S. Masoudpanah, M. Adeli, M. Aboutalebi and M. Habibollahzadeh, Mesoporous honeycomb-like ZnO as ultraviolet photocatalyst synthesized via solution combustion method, *Mater. Res. Bull.*, 2019, **117**, 72–77.

57 Y. Wang, X. Zhang and C. Hou, Facile synthesis of Al-doping 1D ZnO nanoneedles by co-precipitation method for efficient removal of methylene blue, *Nano-Struct. Nano-Objects*, 2018, **16**, 250–257.

58 A. Torane, A. Ubale, K. Kanade and P. Pagare, Photocatalytic dye degradation study of TiO_2 material, *Mater. Today: Proc.*, 2021, **43**, 2738–2741.

59 R. Rescigno, *et al.*, Photocatalytic activity of P-doped TiO_2 photocatalyst, *Photochem. Photobiol. Sci.*, 2023, **22**(6), 1223–1231.

60 Y. Wang, T. Zhang, Y. Zhao, T. Lv, W. Liu and X. Liu, Catalytic degradation of methylene blue by biosynthesized Au nanoparticles on titanium dioxide (Au@TiO_2), *Environ. Sci. Pollut. Res.*, 2023, **30**(5), 12307–12316.

61 Y. Haldorai, R. S. Kumar, S. Ramesh, R. R. Kumar and W. Yang, Sol-gel synthesized CuO nanoparticles supported on reduced graphene oxide nanocomposite for sunlight-catalytic methylene blue degradation and nanofluid applications, *J. Sol-Gel Sci. Technol.*, 2024, **111**(3), 689–702.

62 S. P. Mardikar, S. Kulkarni and P. V. Adhyapak, Sunlight driven highly efficient degradation of methylene blue by CuO–ZnO nanoflowers, *J. Environ. Chem. Eng.*, 2020, **8**(2), 102788.

63 D. K. Harijan, S. Gupta, S. K. Ben, A. Srivastava, J. Singh and V. Chandra, High photocatalytic efficiency of α-Fe_2O_3-ZnO composite using solar energy for methylene blue degradation, *Phys. B*, 2022, **627**, 413567.

64 B. R. Shah and U. D. Patel, Mechanistic aspects of photocatalytic degradation of Lindane by TiO_2 in the presence of Oxalic acid and EDTA as hole-scavengers, *J. Environ. Chem. Eng.*, 2021, **9**(4), 105458.

65 T. H. Jeon, *et al.*, Ag (I) ions working as a hole-transfer mediator in photoelectrocatalytic water oxidation on WO_3 film, *Nat. Commun.*, 2020, **11**(1), 967.